Enhancement of Collapse-Resistant Capacity of Non-Seismically Designed RC Frames using Various CFRP Strengthening Schemes

Shi-Lin Liang[1], Feng Fu[2,3] Zhi-Qiang Huang[4], and Kai Qian[3,*]

[1] College of Civil and Transportation Engineering at Hohai University, Nanjing, 210098, China.

[2] Department of Engineering, School of Science and Technology, City, University of London, EC1V 0HBU.K.

[3] Guangxi Key Laboratory of Green Building Materials and Construction Industrialization, Guilin University of Technology, Guilin, China, 541004.

[4] College of Civil Engineering and Architecture at Guangxi University, Nanning, 531004, China.

Abstract

The existing studies have demonstrated relatively weak robustness of non-seismically designed reinforced concrete (RC) frames against collapse than seismically designed RC frames, causing the demand of efficient strengthening schemes to enhance their collapse-resistant capacity. Therefore, this paper presents an experimental program aiming at strengthening the collapse-resistant capacity of non-seismically designed RC frames using carbon fiber reinforced polymer (CFRP). A total of seven sub-frames were tested, of which the penultimate column or edge column was notionally removed to replicate the initial damage caused by accidental loads. Two sub-frames without strengthening were tested first as reference tests. Similar to existing research outcomes, the referential sub-frames experienced premature rebar fracture at the beam ends near the removed column, resulting in a severe softening in load resistance. Whilst the load resistance could reascend, the fracture of the rebar at the beam ends near the side columns only allowed an insufficient mobilization of catenary action (CA). In addition, the side joint of the referential sub-frame representing a penultimate column removal scenario suffered significant damage. Subsequently, five strengthening schemes were applied to the referential sub-frame, they are designed to increase the compressive arch action (CAA) capacity or CA capacity, or both the CAA and CA capacities through CFRP strengthening. Test results demonstrated that the proposed strengthening schemes in this paper can efficiently increase the load resistance at the CAA and CA stages but failed to mitigate the severe load resistance softening. The strengthening scheme planned to increase the CAA capacity unexpectedly decreased the deformation capacity of the strengthened sub-frame due to premature fracture of beam rebar near the side columns. The strengthening schemes planned to increase the CA capacity or both the CAA and CA capacities could increase not only the CAA capacity but also the CA capacity. The enhanced load resistance at the CA stage was mainly attributed to the continuous CFRP strips attached to the soffits. Unfortunately, the energy method demonstrated that the dynamic load resistance of the tested sub-frames to prevent collapse was achieved at the CAA stage rather than the CA stage because of the severe load resistance softening. Thus, the efforts devoted to increasing the CA capacity by this paper were valid in a real collapse of building scenario. In addition, 113 available test results were collected to compare with the acceptance criteria in existing codes for collapse-resistant design. Based on the test results and comparison, design suggestions were given for the collapse-resistant design.

Keywords: Collapse-resistant; Non-seismically design; Reinforced concrete; CFRP; Strengthening schemes

*Corresponding author. E-mail address: qiankai@glut.edu.cn

1. Introduction

Progressive collapse is defined as ‘‘the spread of an initial local failure from element to element, eventually resulting in the collapse of an entire structure or a disproportionately large part of it’’[1]. The initial local failure of the structural element can be caused by various extreme occasional loads, such as blast, impact, and fire. However, the state of the art of collapse-resistant design of buildings neglects the type and intensity of the occasional loads but introduces the “Alternative load path method” by investigating column removal scenario to assess the performance of the damaged building to bridge the initial local failure. In this case, the internal forces of the structural elements above the removed column can be well beyond the design envelope, which necessitates the mobilization of secondary load transfer mechanisms to resist collapse.

To date, extensive tests have been conducted to demonstrate the behavior of reinforced concrete (RC) frames under the column removal scenario [2-7]. It was found that pure flexural action is always able to develop at the initial loading stage, and then compressive arch action (CAA) begins to dominate the load transfer once sufficient axial constraints are applied to the beam ends. Otherwise, only the pure flexural action can be activated, such as in the case under a corner column removal scenario [8, 9]. The development of CAA is associated with the beam axial compression force and the CAA capacity is found to be mainly related to concrete compressive strength, longitudinal reinforcement ratio, and span/depth ratio of the beam. The enhancement ratio of CAA, which is defined as the ratio of CAA capacity to yield load (YL) capacity, increases nearly linearly with the increase of compressive strength of concrete but decreases with the increase of mechanical reinforcement ratio, and it is the most sensitive to span/depth ratio of the beam [5, 7, 10, 11]. After the CAA stage, a transition stage can occur prior to the CA stage, during which the beam axial compression force begins to convert to axial tension force. The CA can be activated or not is highly dependent on the rotational capacity of the beam ends and boundary conditions (performance of side joint and side column), the former affects the development level of CA while the latter determines the material property of the beam longitudinal rebar can be sufficiently utilized or not. For example, in FarhangVesali et al. [5] and Vali pour et al. [10]'s tests, the beam tension rebar at both beam ends of a beam successively fractured at the CAA stage, consequently, the beam rotated freely because the rotational constraints at the beam ends were released, resulting in a severe load softening after the CAA stage and subsequent limited development of CA. In addition, shear failure of the side beam-column joints [3, 12-14] and large eccentric compression failure of the side columns [15-17] can prevent the sufficient mobilization of CA. It is worthwhile noting that the majority of sub-frames in these tests are non-seismically designed, indicating the relatively weak collapse-resistant capacity of non-seismically designed RC frames, which calls for efficient strengthening schemes to improve their robustness.

Using externally bonded carbon/glass fiber reinforced polymer (CFRP/GFRP) strips or sheets is an effective way to enhance the performance of RC components [18-21]. Karayannis and Golias [18] and Golias et al. [19] used CFRP ropes as external reinforcements to strengthen the RC beam-column joints and found that the strengthened joints exhibited improved structural performance. Chalioris et al. [20] and Kakaletsis et al. [21] summarized the techniques for strengthening RC components, such as the utilization of CFRP U-shaped jackets and plates. In recent years, CFRP/GFRP materials have been employed to strengthen the collapse-resistant capacity of RC structures [22-27]. Kim et al. [23] applied CFRP strips to the side or soffit of the beams for providing continuity to the beams, it was found that both CFRP anchors and CFRP U-wraps can efficiently anchor the CFRP strips. Qian and Li [24] and Feng et al. [26] investigated the merits of externally bonded GFRP strips to enhance the performance of RC beam-slab sub-structures subjected to an interior and a corner column missing scenario, respectively. Liu et al.

[25] adopted CFRP cables to retrofit the collapse-resistant capacity of a 1/2 scale RC structure. It was found that the RC structure could obtain a new balance after the sudden loss of two edge columns. Elsanadedy et al. [27] used CFRP U-wraps to strengthen the dry connections of the precast concrete sub-frame, it was found that the upgraded sub-frame had a similar ultimate load capacity to the RC sub-frame.

To enhance the collapse-resistant capacity of non-seismically designed RC frames using CFRP strengthening technique, an experimental program including two referential RC sub-frames and five strengthened RC sub-frames with CFRP is conducted in this paper. The strengthening schemes aim to increase either CAA capacity or CA capacity, or both the CAA and CA capacities. In addition, available test results in terms of the plastic rotations of the beam ends are collected to compare with the acceptable performance criteria in existing codes for collapse-resistant design. Based on the test results and comparative study, design recommendations for collapse-resistant design of RC buildings were made.

2. Experimental Program

2.1 Sub-frame design and material property

The design of the prototype RC building follows the building code ACI 318-19 [28]. The design dead load and live load are 5.5 kPa and 2.0 kPa, respectively. Seven sub-frames were extracted from the prototype building and scaled down to 1/2 as specimens for test. The information on the experimental program is listed in **Table 1**. The sub-frames are categorized into two groups based on the removed columns. Group 1 consists of three sub-frames under the loss of a penultimate column (P-R, P-S-C, and P-S-CC) whereas Group 2 includes four sub-frames subjected to the loss of an edge column (E-R, E-S-C, E-S-CC1, and E-S-CC2). In the notations of sub-frames, the first letter P or E denotes the removed columns; the second letter R or S indicates referential or strengthened sub-frames; the third letter C and the fourth letter C (if any) mean CAA and CA, respectively. The geometric dimension and reinforcement arrangement of the sub-frames are shown in **Fig. 1**. The beam was 2750 mm in length. The sectional dimensions of the beam and the column were 150 mm×250 mm and 250 mm×250 mm, respectively. Ribbed reinforcing bars with diameters of 10 mm (T10) and 12 mm (T12) were used as the longitudinal rebar of the beams and columns, respectively. Round bars with a diameter of 6 mm and a spacing of 100 mm were arranged along the beams. The beams were extended from both side joints for the sub-frames subjected to the edge column removal scenario. The extended beams were designed to simulate the axial constraints from adjacent bays. In contrast, sub-frames under the penultimate column removal scenario were in asymmetric boundary conditions, only the beam on the left side was extended from the side joint. Compared with seismically designed frames, the frames studied here had relatively lower reinforcement ratio. Moreover, the sum of flexural strengths of columns shall be greater than 1.2 times the sum of flexural strengths of the beams for seismically designed frames (ACI 318-19 [28]). However, in this study, the ratio of the sum of flexural strengths of columns to the sum of flexural strengths of the beams was 1.1.

Table 2 lists the material properties of the reinforcement and CFRP. The concrete used to cast the sub-frames has an average cylinder compressive strength of 36.4 MPa and an average splitting tensile strength of 3.3 MPa. In addition, the maximum aggregate size of the concrete is 10 mm.

2.2 Test setup and instrumentation

Fig. 2 shows the test setup. The test setup and installation of the two groups of sub-frames are similar. The top of the side column and the extended beam were linked to the reaction frame via horizontal constraints, the side column base was pinned to the strong ground of the laboratory. The targeted column was notionally removed before testing. Hydraulic jack 1 (Item 3) and a steel assembly (Item 5) were installed to ensure in-plane loading of the sub-frames. To account for the effect of gravity load from the upper stores, hydraulic jack 2 (Item 7) was installed to implement an axial compression ratio of 0.2 to the side columns. At the beginning of the test, constant axial compression was first applied to the side columns, and then a displacement-control loading scheme was used to apply load to the top of the target column by the hydraulic jack with a loading rate of 0.5 mm/min.

Two load cells (Items 2 and 4) were installed along the axis of hydraulic jack 1 to measure the load applied to the sub-frames. Tension/compression load cells and load pins were installed in the horizontal constraints and pin supports to monitor the horizontal reaction forces. In addition, a series of seven linear variable displacement transducers (LVDTs, Item 6) were arranged along the length of the beams to record the deflection of the beams; another series of ten LVDTs (Item 9) were installed along the height of the two side columns to record their horizontal movement. Moreover, strain gauges were mounted to the reinforcement and CFRP strips.

3. Test Results of Referential Sub-frames

3.1 Load resistance and failure mode

Fig. 3a shows the load resistance-displacement history of the referential sub-frames while **Table 3** lists the critical test results. The overall trend of the load resistance-displacement history was consistent with the results from available tests of non-seismically designed RC sub-frames [3, 10, 13]. The load resistance was dominated by the CAA capacity. A severe load resistance softening occurred after the CAA capacity, after which was a limited development of CA. The YL/CAA capacities of P-R and E-R were 33 kN/42 kN and 35 kN/45 kN, respectively. Therefore, the enhancement ratios of CAA were 1.27 and 1.29, respectively. The first rebar fracture occurred in the beam bottom rebar near the removed column at the displacements of 125 mm and 150 mm for P-R and E-R, respectively. Then, consecutive fracture of the tension rebar of beam ends was measured. Accordingly, the load resistance of the two sub-frames decreased continuously as the beam ends lost the bending moment capacity. The load resistance gained a limited increase because of CA. However, the CA capacities of P-R and E-R were 33 kN and 40 kN, respectively, less than the CAA capacities.

Fig. 4 and **Fig. 5** show the failure modes of P-R and E-R, respectively. The beam tension rebars at the beam ends were fractured except that of the beam end near the left-side column. The distributed cracks along the beams indicated that the beams were in tension at the end of the tests. Moreover, hairline flexural cracks were formed in the exterior side of the side columns because the axial compression of the beam at the CAA stage pushed the side column to move outward. Different from ER, extensive cracks were formed in the right-side column of PR at the CA stage due to the absence of the extended beam.

3.2 Horizontal reaction force

Fig. 6a illustrates the horizontal reaction force-displacement relationship of P-R and E-R. Horizontal compressive reaction forces (HCRF) were first measured. The maximum HCRFs on the left side and right side of PR were -76 kN and -61 kN, respectively. Therefore, the presence of the extended beam could increase the maximum HCRF by 24.6%. The maximum HCRF of ER was -82 kN, which was 7.9% greater than that of PR. When the rebar fractured at the CAA stage, the HCRF only experienced a mild variation. When the CA kicked in, the HCRF converted to horizontal tensile reaction force (HTRF). The maximum HTRFs on the left side and right side of P-R were 90 kN and 73 kN, respectively. The maximum HCRF of E-R was 102 kN, which was 13.3% greater than that of P-R.

3.3 Deflection of the beam and side column

Fig. 7 demonstrates the deflection of the beam of E-R. It can be seen that the beams exhibited visible flexural deformation at the beam ends whereas the middle segment of the beams almost kept straight. At the final of the test, the deflection shape of the left side beam was similar to a cantilever beam because the beam end near the left side column was still able to sustain bending moment. Differently, since the beam tension rebar of the beam ends fractured completely, the whole right-side beam kept straight. Similar observation was obtained in P-R. **Fig. 8** compares the deflection of the right-side column (without extended beam) of E-R and P-R. The side column moved outward at the CAA stage because of the axial compression in the beams. Afterward, the side columns began to move inward to respond to the axial tension of the beams at the CA stage. The maximum outward movements of the right-side column of E-R and P-R were -5.1 mm and -6.5 mm, respectively, whereas the maximum inward movements were 5.4 mm and 7.6 mm, respectively.

4. Strengthening Schemes

Based on the test results of the referential sub-frames, the main weaknesses of non-seismically designed RC frames under a column removal scenario are summarized as follows: (1) relatively low beam reinforcement ratio leads to the premature fracture of the beam rebar at the CAA stage, which in turn results in a severe load softening; (2) due to the same reason, the CA gains limited development; (3) the exterior beam-column joint (without constraint from the extended beam) can suffer severe damage. Therefore, five strengthening schemes with CFRP were developed in this paper to improve their collapse-resistant capacity, as shown in **Fig. 9**. The number in **Fig. 9** indicates the construction steps. The strengthening schemes were designed in accordance with ACI 440.2R-17 [29], the details of each strengthening scheme was presented below.

4.1 P-S-C

Fig. 9a demonstrates the strengthening scheme of P-S-C. This sub-frame was strengthened to achieve a higher CAA capacity. First, L-shaped CFRP strips with a branch length of 500 mm were applied to the beam ends and columns. It should be noted that the 500 mm length was designed considering the length of potential plastic hinge was 250 mm (one beam depth) and the additional length of 250 mm for anchorage. The anchorage length of 250 mm was greater than the requirement of ACI 440.2R-17 [29]. A straight CFRP strip with 1250 mm in length and 150 mm in width was applied on the exterior face of the right side column to enhance the bending moment capacity of the beam ends and columns (Item ①); Second, CFRP wraps were applied to the columns with a spacing of 150 mm for enhancing the columns and providing anchorage to the L-shaped strips (Item ②); Third, CFRP strips with 200 mm in height were applied to the side of beam-column joints to improve the shear strength of joints (Item ③, not reaching the height of the beam considering the presence of slabs in practical buildings); Fourth, U-shaped CFRP wraps with 150 mm in width were applied to the beam ends to enhance the anchorage of the horizontal branch of the L-shaped CFRP strips as suggested by Kim et al. [23] (Item ④). Both the CFRP strips and wraps were two layers, and epoxy was used for bonding CFRP.

4.2 P-S-CC

As shown in **Fig. 9**b, on the basis of the strengthening scheme of P-S-C, additional two layers of continuous CFRP strips were first applied to the soffit of the beams of P-S-CC for providing continuity, which was expected to be able to enhance the CA capacity. To ensure continuity, the CFRP strips were divided by two at the beam-column interfaces and threaded through two pre-drilled holes in the columns, as suggested by previous studies [22, 23].

4.3 E-S-C

E-S-C was strengthened to obtain a higher CA capacity. As shown in **Fig. 9**c, the continuous CFRP strips were applied to the soffit of the beams, and U-shaped CFRP wraps were applied to the beam ends to prevent the delamination of the continuous CFRP strip.

4.4 E-S-CC1 and E-S-CC2

The strengthening schemes of E-S-CC1 and E-S-CC1 are shown in **Fig. 9**d. The strengthening details of E-S-CC1 were similar to that of P-S-CC. However, for E-S-CC2, the L-shaped CFRP strips, U-shaped CFRP wraps, and CFRP strips on the side of the beam-column joints were changed to one layer. Moreover, the CFRP warps on the columns were changed to three layers.

5. Test Results of Strengthened Sub-frames

5.1 Load resistance and failure mode

P-S-C and P-S-CC

The load resistance-displacement histories of P-S-C and P-S-CC are shown in **Fig. 3**b and the critical test results are listed in **Table 3**. It can be seen that the overall trend of the load resistance-displacement histories of P-S-C and P-S-CC was similar to that of P-R. Compared with P-R, the YL capacities of P-S-C and P-S-CC were increased by 21.2% and 33.3%, namely, 40 kN and 44 kN, respectively. Moreover, the CAA capacities of P-S-C and P-S-CC were increased by 16.7% and 23.8%, i.e., 49 kN and 52 kN, respectively. However, severe load softening also occurred in P-S-C and P-S-CC, in particular for P-S-C. Different from P-R, for P-S-C, the first rebar fracture occurred in the beam top rebar near the right-side column at a displacement of 183 mm. Subsequently, consecutive fracture of the tension rebar of the beam ends was observed. As a result, the L-shaped CFRP strips began to de-bond and the CFRP wraps on the column ruptured. At a displacement of 290 mm, the beam bottom rebar near the removed column fractured completely, resulting in debonding of L-shaped strips, which in turn led to the rupture of the overlying CFRP wraps on the removed column. Consequently, the beam ends of P-S-C could not sustain bending moment anymore, and the load resistance within the displacement from 280 mm to 310 mm was closed to zero. The load resistance of P-S-C could reascend but drop to zero after reaching the CA capacity of 24 kN, which was 27.3% less than that of P-R. For P-S-CC, the CAA capacity was followed by an immediate drop in load resistance, which was ascribed to the slight debonding of the continuous CFRP strip near the removed column. The beam bottom rebar near the removed column fractured first at a displacement of 172 mm. However, the continuous CFRP strip prevented the complete fracture of beam bottom rebar near the removed column, therefore, P-S-CC did not lose its load resistance even though the beam top rebar near the side columns fractured completely. At the final, partial continuous CFRP strip near the removed column was ruptured. The CA capacity of P-S-CC of 55 kN was achieved at a displacement of 621 mm, which was 66.7% greater than that of P-R.

Fig. 10 and **Fig. 11** show the failure modes of P-S-C and P-S-CC, respectively. Extensive cracks penetrated the beams depth, rebar fracture occurred at the beam ends, side CFRP strips were ruptured, L-shaped CFRP strips suffered debonding and caused the rupture of the overlying CFRP wraps on the columns. The beam rebar of the beam end near the right-side column fractured completely for P-S-C, but not for P-S-CC due to the present continuous CFRP strip. In addition, the distribution of the cracks along the beams of P-S-CC was sparser than P-S-C. Compared with the failure mode of P-R (**Fig. 4**), the side columns of P-S-C and P-S-CC suffered much milder damage, in particular for the right side column, only one crack was observed.

E-S-C, E-S-CC1, and E-S-CC2

The load resistance-displacement histories of E-S-C, E-S-CC1, and E-S-CC2 are shown in **Fig. 3**c. The YL capacities of E-S-C, E-S-CC1, and E-S-CC2 were 36 kN, 47 kN and 42 kN, respectively, corresponding to the increasements of 2.9%, 34.3%, and 20.0% compared with E-R, respectively. The CAA capacities of E-S-C, E-S-CC1, and E-S-CC2 were 47 kN, 58 kN and 53 kN, respectively, corresponding to the increasements of 4.4%, 28.9%, and 17.8% compared with E-R, respectively. For E-S-C, the beam bottom rebar near the removed column was first to fracture at a displacement of 193 mm. The test of E-S-C was stopped due to consecutive fracture of beam top rebar near the side column. The CA capacity of 46 kN was measured at a displacement of 567 mm, which was 15.0% greater than that of E-R. E-S-CC1 and E-S-CC2 obtained their CA capacities of 58 kN and 49 kN at the displacement of 597 mm and 577 mm, respectively, which were 145.0% and 122.5% of that of E-R, respectively.

Fig. 12, **Fig. 13**, and **Fig. 14** give the failure modes of E-S-C, E-S-CC1, and E-S-CC2, respectively. In general, the failure mode of E-S-C was similar to that of E-R except that more cracks formed in the side column because of the additional tensile force from the continuous CRFP strip. The failure mode of E-S-CC1 was analogous to that of P-S-CC: extensive cracks developed along the beams, rebar fracture occurred at the beam ends, L-shaped CFRP strips suffered debonding and the overlying CFRP wraps on the columns were ruptured. However, no debonding occurred in the L-shaped CFRP strip of E-S-CC2, and the CFRP wraps were intact at the end of test. This is because both the L-shaped CFRP strips and CFRP wraps on columns of E-S-CC1 were two layers, whereas the L-shaped CFRP strips and CFRP wraps on columns of E-S-CC2 were one layer and three layers, respectively.

5.2 Horizontal reaction force

The horizontal reaction force-displacement curves of the strengthened sub-frames are shown in **Fig. 6**. The left/right side maximum HCRFs of P-S-C and P-S-CC were -91/-78 kN and -98/-85 kN, respectively, indicating the increasements of 19.7/27.9% and 28.9/39.3% compared with P-R, respectively. The maximum HTRFs of P-S-C and P-S-CC were 67/58 kN and 125/113 kN, respectively. Therefore, P-S-C obtained the lowest maximum HTRF, which agreed well with the load resistance. The maximum HCRFs of E-S-C, E-S-CC1, and E-S-CC2 were -87 kN, -111 kN, and -101 kN, respectively.

Compared with E-R, the maximum HCRFs of E-S-C, E-S-CC1, and E-S-CC2 were higher by 6.1%, 35.4%, and 23.2%, respectively. The maximum HTRFs of E-S-C, E-S-CC1, and E-S-CC2 were 111 kN, 138 kN, and 119 kN, respectively, which were 8.8%, 35.3%, and 16.7% higher than that of E-R, respectively.

5.3 Strain of CFRP strips

Fig. 15 presents the strains of the CFRP strips of P-S-C and P-S-CC at the stage of CAA. The strain of the CFRP strip bonded on the exterior face of the right-side column was in tension as a result of the outward deflection of the side column due to beam compressive axial force. Besides, the CFRP strips were proved to have been properly bonded on the tensile zone of the beam ends since considerable tensile strain developed there, confirming the effectiveness of the proposed strengthening schemes for improving the flexural capacity of beams. Similar results were obtained for other specimens.

6. Discussion

6.1 Efficiency of the strengthening schemes

As tabulated in **Table 3**, the YL/CAA/CA capacities of P-R, P-S-C, and P-S-CC were 33/42/33 kN, 40/49/24 kN, and 44/52/55 kN, respectively. Compared with the referential sub-frame P-R, the YL/CAA/CA capacities of P-S-C and P-S-CC were increased by 21.2%/16.7%/-27.3% and 33.3% /23.8%/66.7%, respectively. Therefore, the strengthening schemes effectively enhance the collapse-resistant capacity of P-S-C and P-S-CC at the YL and CAA stages. However, P-S-C achieved the lowest CA capacity among these three sub-frames, this will be discussed below. The YL/CAA/CA capacities of E-R, E-S-C, E-S-CC1, and E-S-CC2 were 35/45/40 kN, 36/47/46 kN, 47/58/58 kN, and 42/53/49 kN, respectively, which were 2.9%/4.4%/15.0%, 34.3% /28.9%/45.0%, and 20.0% /17.8%/22.5% higher than that of the referential sub-frame E-R, respectively. The deformation capacity, which was defined as the displacement at CA capacity, of P-R, P-S-C, and P-S-CC was 552 mm, 560 mm, and 621 mm, respectively. The strengthening scheme aiming at increasing CAA capacity had a marginal effect on the deformation capacity of the sub-frame subjected to a penultimate column removal scenario whereas the strengthening scheme designed to enhance both CAA and CA capacity increased the deformation capacity by 12.5%. The deformation capacity of E-R, E-S-C, E-S-CC1, and E-S-CC2 was 532 mm, 567 mm, 597 mm, and 577 mm, respectively. The strengthening scheme aiming at increasing CA capacity increased the deformation capacity of the sub-frame subjected to an edge column removal scenario by 6.6% whereas the strengthening scheme designed to improve both CAA and CA capacity increased the deformation capacity by 8.5% to 12.2%.

In summary, the strengthening schemes could effectively improve the collapse-resistant capacity of the sub-frames. However, as shown in **Fig. 3**, the load resistance of the strengthened sub-frames at the transition stage is even lower than that of the referential sub-frames, indicating that the strengthening schemes failed to alleviate the severe load resistance softening. This is because the application of CFRP resulted in the strain concentration at the beam ends, and the detrimental influence of the strain localization aggravated the premature fracture of beam rebar. In this case, P-S-C obtained the lowest CA load resistance and deformation capacity. However, sub-frames with continuous CFRP strip were capable of further developing CA.

Compared with P-R, the fewer cracks in the right-side columns of P-S-C and P-S-CC demonstrated that the CFRP wraps could mitigate the damage to the columns. The L-shaped CFRP strips experienced debonding and resulted in the rupture of the overlying CFRP wraps on the columns for the strengthened sub-frames except for E-S-CC2. In contrast, for E-S-CC2, the L-shaped CFRP strips were fractured whereas the CFRP wraps were intact. In this study, the CFRP wraps were used to provide anchorage to the L-shaped CFRP strips, and therefore, the failure mode of E-S-CC2 was more preferent. In E-S-CC2, the layer number of the CFRP wraps was three times that of the L-shaped CFRP strips. However, the layer number of the CFRP wraps and the layer number of the L-shaped CFRP strips in the other strengthened sub-frames were equal.

6.2 Dynamic collapse-resistant capacity

The static load resistance recorded in the test shall be transformed into the dynamic load resistance due to the dynamic nature of progressive collapse. In this section, the transformation was implemented with the energy-based framework proposed by Izzuddin et al. [30]. As illustrated in **Fig. 16**, the strain energy W_s in the remaining structure in the event of zero kinetic energy is equal to the work W_g done by the concentrated load. Thus, the pseudo-static load resistance, i.e., dynamic load resistance, can be obtained by dividing the area under the measured quasi-static load-displacement curve by the displacement. **Fig. 17** shows the dynamic collapse-resistant capacities of the sub-frames. The peak dynamic collapse-resistant capacities of P-R, P-S-C, P-S-CC, E-R, E-S-C, E-S-CC, and E-S-CC2 were

35 kN, 44 kN, 43 kN, 39 kN, 41 kN, 51 kN, and 46 kN, respectively. It can be seen that the overall trend of dynamic load resistance-displacement histories of the sub-frames was different from that of static ones. The peak dynamic load resistances were attained at the CAA stage, and no obvious reascending behavior was observed after the load resistance softening. Therefore, whilst the CA capacities of P-S-CC and E-E-S-CC2 were higher than the CAA capacities, their peak dynamic collapse-resistant capacities were achieved at the CAA stage. This is because the severe load resistance softening could result in an appreciable amount of kinetic energy of the beams during collapse while the development of CA was too limited to consume all the kinetic energy. Therefore, it was concluded that the strengthened CA capacity failed to increase the dynamic collapse-resistant capacity, however, it can change the collapse mode of buildings due to increased energy dissipation capacity. Moreover, DoD [31] suggests that the use of composite materials such as FRP to provide the tie forces is acceptable when the FRP can meet the rotation requirement of 0.20 rad. However, although the rotational capacity of the beams of P-S-CC, E-S-CC1, and E-S-CC2 exceeded 0.2 rad, test results indicated that no reliable tie force was achieved .

6.3 Acceptable performance criteria for collapse-resistant design

DoD [31] and GSA [32] provide acceptable performance criteria (plastic rotation of beam end $[\theta]$) for RC beams governed by flexural behavior at the collapse prevention level. The acceptance criteria depend on the indicators $(\rho-\rho')/\rho_{\mathrm{bal}}$, $V/b_{\mathrm{w}}d\sqrt{f_c^{'}}$, and the ratio of stirrup spacing to effective beam depth, where ρ, ρ' and ρ_{bal} are tension, compression, and balanced reinforcement ratios of beam critical section, respectively; V is design shear force; b_{w} and d are web width and effective depth of beam; $f_c^{'}$ is compressive strength of concrete. The beams are categorized into conforming and nonconforming (C and NC) beams depending on the hoop spacing within the plastic hinge region. If the hoops are spaced at ≤d/3, the beams are conforming, otherwise, nonconforming. The C and NC beams can be approximately considered seismically and non-seismically designed beams, respectively, because the maximum hoop spacing of seismically designed beams is explicitly required to be less than or equal to d/4 [28, 33]. The acceptance criteria for primary and secondary components are different for DoD [31], but not for GSA [32]. In DoD [31], stricter acceptance criteria are stipulated for the primary component. In GSA [32], the acceptance criteria of the primary and secondary components are the same and are equal to the acceptance criteria of the secondary component in DoD [31]. More details can be found in Table 6 in GSA [32] and Table 4-1 in DoD [31].

To assess the acceptable performance criteria for collapse prevention, a database including 113 test results was built based on available papers to conduct a comparative study [2-5, 7, 9-13, 34-49]. The information on the collected tests is listed in **Table 4**. Since the information on the design loads was not provided in many papers, the indicator $V / b_w d \sqrt{f_c^{'}}$ was taken less than or equal to 0.25, units in MPa. As shown in **Table 4**, the measured plastic rotation of the beam end at the CAA capacity θ_{CAA}, which was determined by subtracting the chord rotation of the beam at the YL capacity θ_y from the θ_{CAA}, was compared with the acceptance criteria. The chord rotation of the beam is defined as the ratio of removed column displacement to beam's clear span. For the tests without information about YL, the measured θ_{CAA} was approximately determined by the chord rotation of the beam at the CAA capacity. As listed in **Table 4** and **Fig. 18**, the measured θ_{CAA} fall in the acceptable range of both GSA [32] and DoD [31]. In other words, the CAA is supposed to be a reliable defense line against collapse.

The above acceptable performance criteria at the collapse prevention level are for RC beams controlled by flexure, which means the collapse of building is preferred to be prevented at flexural stage. However, this may be too conservative if considerable CA can be developed in the beams. The beams undergoing CA, which transfer the loads from the damaged region of the building to the undamaged portion via tie forces rather than flexure, are controlled by axial tensile force. To date, related acceptable performance criteria are not clear. DoD [31] stipulates that unless the beams and their connections can be shown capable of carrying the required tie force while undergoing rotations of 0.2 rad, the tie forces are to be carried by the floor and roof system. Among the 113 tests, only 55 tests (48.7%) demonstrated a superior CA capacity to CAA capacity. As shown in **Fig. 19**, in general, the beams in these 55 tests were able to provide 0.2 rads. In other words, 0.2 rad rotational capacity of the beams can ensure considerable CA capacity. Unfortunately, no explicit method is available to judge whether the beams can provide 0.2 rads due to various influential parameters.

In reality, the conclusions on the reliability of CA to work as the second defense line to resist collapse are inconsistent owing to different specimens. Yu and Tan [7] and Yu and Tan [13] conducted tests of RC beam-column assemblies with similar geometric dimensions and reinforcing details but different side columns, the former used simplified enlarged side columns, whereas the latter adopted scaled side columns, similar to the current study. It was found that, due to the absence of axial compression in the side columns, the simplified enlarged side columns can result in overestimated rotational capacity of the beam ends near the side columns and CA capacity. In comparison, the rotational capacity of the beam ends of assemblies with scaled side columns was less. This is because the axial compression ratios of 0.4 to 0.6 of the scaled side columns put the longitudinal rebar of the beams in a higher bond stress regime, which resulted in premature rebar fracture and lower CA capacity. However, in Qian et al. [47] and Qian et al. [49]'s tests, comparable rotational capacities of the beam ends and CA capacities were measured for the assemblies with simplified enlarged side columns and scaled side columns, which may be attributed to the relatively lower axial compression ratio of 0.3 of the scaled side columns. Moreover, the development of CA depends on boundary conditions, reinforcement ratio, and span-to-depth ratio of the beams, which are various in buildings. In summary, it is reasonable to exclude CA from the acceptable load-resisting mechanism to mitigate collapse until explicit method for determination of the rotational capacity of beams is proposed.

6.4 A simple collapse-resistant design method

To improve the current collapse-resistant design, a simple design method was proposed, which included two steps: First, determining the load resistance function of critical components of the target frame, i.e., sub-frame; Second, determining the dynamic collapse-resistant capacity based on the load resistance function. As shown in **Fig. 20**, the load resistance function was assumed to be trilinear and featured three key points: points (d_y, P_y), (d_{CAA}, P_{CAA}), and (d_u, P_u). P_y, P_{CAA}, and P_u indicate YL, CAA capacity, and ultimate load at the acceptable performance criterion, respectively, and d_y, d_{CAA}, and d_u indicate the displacement at YL, CAA capacity, and ultimate load, respectively. The load resistance after the acceptable performance criterion was neglected to obtain a conservative design. P_y is calculated by **Eq. 1**. The nominal flexural strength of the beam section M_y can be calculated by **Eq. 2** [50].

$$P_{\mathrm{y}} = \frac{2(M_{\mathrm{y1}} + M_{\mathrm{y2}})}{l_{\mathrm{n}}} \tag{1}$$

$$M_{\mathrm{y}} = \rho f_{\mathrm{y}} d^2 (1 - 0.59 \rho f_{\mathrm{y}} / f_{\mathrm{c}}) \tag{2}$$

$$d_{\mathrm{y}} = \frac{M_{\mathrm{y}}}{0.3 E_{\mathrm{c}} I} l_{\mathrm{n}} \tag{3}$$

where M_{y1} and M_{y2} are the nominal flexural strengths of the two beam ends of a beam; l_n is the clear span of the beam; ρ is the tension reinforcement ratio; f_y is the yield strength of tension reinforcement; d is the effective beam depth; f_c is the cylinder compressive strength of concrete; $0.3E_cI$ is the effective flexural rigidity of RC beam as suggested by ASCE-41 [51]; I is the inertial moment of beam section; and E_c is the elastic modulus of concrete.

An important challenge is to calculate P_{CAA}. For the beams with insufficient axial constraint (YL dominated), like the beams under a corner column removal scenario, P_{CAA} can be taken as P_y. For the beams with sufficient axial constraint (CAA dominated), P_{CAA} can be calculated by existing CAA model [52, 53], and d_{CAA} is suggested to be $0.033l_n$ based on the average value of the measured values of the database. Based on the discussion in Section 6.3, the acceptance criterion was suggested to be 0.063 rad because such a criterion included almost all CAA capacities of the database. Therefore, d_u is calculated as (d_y+$0.063l_n$). P_u can be assumed to be equal to P_y. Based on the determined load resistance function and energy method [30], the dynamic collapse-resistant capacity P_d is obtained as **Eq. 4**. Besides the energy method, single degree of freedom model can be used to conduct nonlinear dynamic analysis to obtain P_d [16, 54].

$$P_{\mathrm{d}}=\frac{0.5P_{\mathrm{y}}d_{\mathrm{y}}+0.5(P_{\mathrm{y}}+P_{\mathrm{CAA}})(d_{\mathrm{CAA}}-d_{\mathrm{y}})+0.5(P_{\mathrm{CAA}}+P_{\mathrm{u}})(d_{\mathrm{u}}-d_{\mathrm{CAA}})}{d_{\mathrm{u}}} \tag{4}$$

7. Conclusions

An experimental program was carried out to enhance the collapse-resistant capacity of non-seismically designed RC frames using various CFRP strengthening schemes. Moreover, existing acceptance criteria for collapse prevention were compared with numerous test results. Based on the test results and discussion, the main conclusions were drawn as follows:

1. The strengthening schemes can effectively enhance the collapse-resistant capacity of P-S-C and P-S-CC at the CAA and CA stages. The YL/CAA/CA capacities of P-S-C and P-S-CC were 21.2%/16.7%/-27.3% and 33.3% /23.8%/66.7% higher than that of the referential sub-frame P-R, respectively. The YL/CAA/CA capacities of E-S-C, E-S-CC1, and E-S-CC2 were 2.9%/4.4%/15.0%, 34.3% /28.9%/45.0%, and 20.0% /17.8%/22.5% higher than that of the referential sub-frame E-R, respectively.

2. On the one hand, the strengthening schemes could increase the collapse-resistant capacity of the sub-frames. On the other hand, the strengthening schemes could aggravate premature rebar fracture due to strain localization of the beams, leading to a higher CAA capacity but lower CA capacity and deformation capacity, such as P-S-C.
3. Whilst the CA capacities of P-S-CC, E-S-C, E-S-CC1, and E-S-CC2 were equal to or higher than their CAA capacities, the dynamic collapse-resistance capacities of these sub-frames were obtained at the CAA stage, indicating that the strengthened CA capacity was unable to increase the dynamic collapse-resistance, which can be attributed to the severe softening of load resistance.
4. The comparison of the acceptance criteria and measured plastic rotations of the beam ends at the CAA capacity demonstrated that CAA is an acceptable mechanism for collapse prevention. If the beams can ensure 0.2 rad rotational capacity, considerable CA capacity can be obtained. However, the lack of methods to determine the rotational capacity of the beams makes CA unreliable in collapse-resistant design.

Acknowledgments

The authors gratefully acknowledge the financial support provided by the National Natural Science Foundation of China (Nos. 51778153 and 52022024). Any opinions, findings and conclusions expressed in this paper do not necessarily reflect the view of the National Natural Science Foundation of China.

References

[1] ASCE-7 ASCE 7-16 Minimum Design Loads and Associated Criteria for Buildings and Other Structures. 2016.

[2] Su YP, Tian Y, Song XS. Progressive collapse resistance of axially-restrained frame beams. ACI Structural Journal 2009;106(5):600-8.

[3] Choi H, Kim J. Progressive collapse-resisting capacity of RC beam–column sub-assemblage. Magazine of Concrete Research 2011;63(4):297-310.

[4] Sadek F, Main JA, Lew HS, Bao YH. Testing and analysis of steel and concrete beam-column assemblies under a column removal scenario. Journal of Structural Engineering 2011;137(9):881-92.

[5] FarhangVesali N, Valipour H, Samali B, Foster S. Development of arching action in longitudinally-restrained reinforced concrete beams. Construction and Building Materials 2013;47:7-19.

[6] Stinger SM, Orton SL. Experimental evaluation of disproportionate collapse resistance in reinforced concrete frames. ACI Structural Journal 2013;110(3):521-9.

[7] Yu J, Tan KH. Structural behavior of RC beam-column subassemblages under a middle column removal scenario. Journal of Structural Engineering 2013;139(2):233-50.

[8] Qian K, Li B. Dynamic performance of RC beam-column substructures under the scenario of the loss of a corner column—Experimental results. Engineering Structures 2012;42:154-67.

[9] Qian K, Li B. Performance of three-dimensional reinforced concrete beam-column substructures under loss of a corner column scenario. Journal of Structural Engineering 2013;139(4):584-94.

[10] Vali pour H, Vessali N, Foster SJ, Samali B. Influence of concrete compressive strength on the arching behaviour of reinforced concrete beam assemblages. Advances in Structural Engineering 2015;18(8):1199-214.

[11] Deng XF, Liang SL, Fu F, Qian K. Effects of high-strength concrete on progressive collapse resistance of reinforced concrete frame. Journal of Structural Engineering 2020;146(6):04020078.

[12] Kang SB, Tan KH. Robustness assessment of exterior precast concrete frames under column removal scenarios. Journal of Structural Engineering 2016;142(12):04016131.

[13] Yu J, Tan KH. Structural behavior of reinforced concrete frames subjected to progressive collapse. ACI Structural Journal 2017;114(1):63-74.

[14] Qian K, Li B. Effects of masonry infill wall on the performance of RC frames to resist progressive collapse. Journal of Structural Engineering 2017;143(9):04017118.

[15] Qian K, Liang SL, Fu F, Fang Q. Progressive collapse resistance of precast concrete beam-column sub-assemblages with high-performance dry connections. Engineering Structures 2019;198:109552.

[16] Qian K, Liang SL, Xiong XY, Fu F, Fang Q. Quasi-static and dynamic behavior of precast concrete frames with high performance dry connections subjected to loss of a penultimate column scenario. Engineering Structures 2020;205:110115.

[17] Qian K, Liang SL, Feng DC, Fu F, Wu G. Experimental and Numerical Investigation on Progressive Collapse Resistance of Post-Tensioned Precast Concrete Beam-Column Subassemblages. Journal of Structural Engineering 2020;146(9):04020170.

[18] Karayannis CG, Golias E. Full-scale experimental testing of RC beam-column joints strengthened using CFRP ropes as external reinforcement. Engineering Structures 2022;250:113305.

[19] Golias E, Zapris AG, Kytinou VK, Kalogeropoulos GI, Chalioris CE, Karayannis CG. Effectiveness of the novel rehabilitation method of seismically damaged RC joints using C-FRP ropes and comparison with widely applied method using C-FRP sheets—Experimental investigation. Sustainability 2021;13(11):6454.

[20] Chalioris CE, Zapris AG, Karayannis CG. U-jacketing applications of fiber-reinforced polymers in reinforced concrete T-beams against shear—Tests and design. Fibers 2020;8(2):13.

[21] Kakaletsis DJ, David KN, Karayannis CG. Effectiveness of some conventional seismic retrofitting techniques for bare and infilled R/C frames. Structural Engineering and Mechanics 2011;39(4):499-520.

[22] Orton S, Jirsa JO, Bayrak O. Carbon fiber-reinforced polymer for continuity in existing reinforced concrete buildings vulnerable to collapse. ACI Structural Journal 2009;106(5):608-16.

[23] Kim I, Jirsa JO, Bayrak O. Use of carbon fiber-reinforced polymer to provide continuity in reinforced concrete beams under dynamic loading. ACI Structural Journal 2015;112(3):383-95.

[24] Qian K, Li B. Strengthening of multibay reinforced concrete flat slabs to mitigate progressive collapse. Journal of Structural Engineering 2015;141(6):04014154.

[25] Liu T, Xiao Y, Yang J, Chen BS. CFRP strip cable retrofit of RC frame for collapse resistance. Journal of Composites for Construction 2017;21(1):04016067.

[26] Feng P, Qiang H, Ou X, Qin W, Yang J. Progressive collapse resistance of GFRP-strengthened RC beam–slab subassemblages in a corner column–removal scenario. Journal of Composites for Construction 2019;23(1):04018076.

[27] Elsanadedy HM, Al-Salloum YA, Alrubaidi MA, Almusallam TH, Siddiqui NA, Abbas H. Upgrading of precast RC beam-column joints using innovative FRP/steel hybrid technique for progressive collapse prevention. Construction and Building Materials 2021;268:121130.

[28] ACI (American Concrete Institute). Building code requirements for structural concrete and commentary. ACI 318-19. Farmington Hills, MI: ACI. 2019.

[29] ACI (American Concrete Institute). Guide for the design and construction of externally bonded FRP systems for strengthening concrete structures. ACI 4402R-17. Farmington Hills, Michigan, ACI Committee 440. 2017.

[30] Izzuddin BA, Vlassis AG, Elghazouli AY, Nethercot DA. Progressive collapse of multi-storey buildings due to sudden column loss—Part I: Simplified assessment framework. Engineering Structures 2008;30(5):1308-18.

[31] DoD (US Department of Defense). Design of buildings to resist progressive collapse: unified facilities criteria (UFC) 4-023-03. Washington DC, US Department of Defense (DoD). 2016.

[32] GSA (US General Services Administration). Progressive collapse analysis and design guidelines for New Federal Office Buildings and major modernization projects. Washington DC, US General Services Administration. 2016.

[33] MOHURD (Ministry of Housing and Urban-Rural Development of the People's Republic of China). Code for design of concrete structures. GB 50010-15. Beijing: China, Architecture & Building Press. 2015.

[34] Yu J, Tan KH. Special detailing techniques to improve structural resistance against progressive collapse. Journal of Structural Engineering 2014;140(3):04013077.

[35] Kang SB, Tan KH. Behaviour of precast concrete beam–column sub-assemblages subject to column removal. Engineering Structures 2015;93:85-96.

[36] Kang SB, Tan KH, Yang EH. Progressive collapse resistance of precast beam–column sub-assemblages with engineered cementitious composites. Engineering Structures 2015;98:186-200.

[37] Qian K, Li B, Ma JX. Load-carrying mechanism to resist progressive collapse of RC buildings. Journal of Structural Engineering 2015;141(2):04014107.

[38] Alogla K, Weekes L, Augusthus-Nelson L. A new mitigation scheme to resist progressive collapse of RC structures. Construction and Building Materials 2016;125:533-45.

[39] Ren P, Li Y, Lu X, Guan H, Zhou Y. Experimental investigation of progressive collapse resistance of one-way reinforced concrete beam–slab substructures under a middle-column-removal scenario. Engineering Structures 2016;118:28-40.

[40] Lim NS, Tan KH, Lee CK. Experimental studies of 3D RC substructures under exterior and corner column removal scenarios. Engineering Structures 2017;150:409-27.

[41] Lim NS, Tan KH, Lee CK. Effects of rotational capacity and horizontal restraint on development of catenary action in 2-D RC frames. Engineering Structures 2017;153:613-27.

[42] Diao MZ, Li Y, Guan H, Lu XZ, Gilbert BP. Influence of horizontal restraints on the behaviour of vertical disproportionate collapse of RC moment frames. Engineering Failure Analysis 2020;109:104324.

[43] Feng FF, Hwang HJ, Yi WJ. Static and dynamic loading tests for precast concrete moment frames under progressive collapse. Engineering Structures 2020;213.

[44] Zhang WX, Wu H, Zhang JY, Hwang HJ, Yi WJ. Progressive collapse test of assembled monolithic concrete frame spatial substructures with different anchorage methods in the beam–column joint. Advances in Structural Engineering 2020;23(9):1–15.

[45] Gu XL, Zhang B, Wang Y, Wang XL. Experimental investigation and numerical simulation on progressive collapse resistance of RC frame structures considering beam flange effects. Journal of Building Engineering 2021;42:102797.

[46] Long X, Wang S, Huang X-J, Li C, Kang S-B. Progressive collapse resistance of exterior reinforced concrete frames and simplified method for catenary action. Engineering Structures 2021;249:113316.

[47] Qian K, Liang SL, Fu F, Li Y. Progressive collapse resistance of emulative precast concrete frames with various reinforcing details. Journal of Structural Engineering 2021;147(8):04021107.

[48] Qian K, Geng SY, Liang SL, Fu F, Yu J. Effects of loading regimes on the structural behavior of RC beam-column sub-assemblages against disproportionate collapse. Engineering Structures 2022;251:113470.

[49] Qian K, Lan DQ, Zhang L, Fu F, Fang Q. Robustness of post-tensioned concrete beam-column subassemblies under various column removal scenarios. Journal of Structural Engineering 2022;148(5):04022032.

[50] Park R, Paulay T. CH4-Strength of Members with Flexure. Reinforced concrete structures. John Wiley & Sons; 2000.

[51] ASCE (American Society of Civil Engineers). Seismic rehabilitation and retrofit of existing buildings. ASCE-41 17 Reston, VA, ASCE-41 17. 2017.

[52] Liang SL, Li Z, Wang CL, Qian K. Experimental and analytical study on the compressive arch action of precast concrete assemblies with monolithic connections to resist progressive collapse. Journal of Structural Engineering 2023;149(4):04023010.

[53] Yu J, Tan KH. Analytical model for the capacity of compressive arch action of reinforced concrete sub-assemblages. Magazine of Concrete Research 2014;66(3):109-26.

[54] Yu J, Yin C, Guo Y. Nonlinear SDOF model for progressive collapse responses of structures with consideration of viscous damping. Journal of Engineering Mechanics 2017;143(9):04017108.

Table 1 Details of the sub-frames

Sub-frame	Element size b×h (mm×mm)		Beam reinforcement				Location of the removed column	Strengthened load transfer mechanism
			Ends		Middle			
	Beam	Column	Top	Bottom	Top	Bottom		
P-R							Penultimate	N/A
E-R							Edge	N/A
P-S-C							Penultimate	CAA
P-S-CC	150×250	250×250	3T10	2T10	2T10	2T10	Penultimate	CAA and CA
E-S-C							Edge	CA
E-S-CC1							Edge	CAA and CA
E-S-CC2							Edge	CAA and CA

Table 2 Material properties of the reinforcement and CFRP

Rebar	Nominal diameter (mm)	Yield strength (MPa)	Ultimate strength (MPa)	Elongation (%)
T12	12	462	596	14.7
T10	10	532	663	12.8
R6	6	368	485	21.0
CFRP	Thickness (mm)	Elastic modulus (MPa)	Ultimate strength (MPa)	Elongation (%)
	0.167	3,467	241,000	1.71

Table 3 Critical test results

Sub-frame	Critical load resistance capacity (kN)			Critical displacements (mm)			L/RMHCRF (kN)	L/RMHTRF (kN)
	YL	CAA	CA	YL	CAA	CA		
P-R	33	42	33	30	70	552	-76/-61	90/73
E-R	35	45	40	20	73	532	-82	102
P-S-C	40	49	24	15	55	560	-91/-78	67/58
P-S-CC	44	52	55	25	64	621	-98/-85	125/113
E-S-C	36	47	46	25	100	567	-87	111
E-S-CC1	47	58	58	25	110	597	-111	138
E-S-CC2	42	53	49	23	60	577	-101	119

Table 4 Database for comparison of the acceptable plastic rotations for collapse prevention with the measured ones

Papers	Specimen ID	Beam clear span (mm)	Critical beam section			$(\rho-\rho')/\rho_{bal}$	Beam type	Critical displacement (mm)		Measured plastic rotation (rad)		$[\theta]$ (rad)		$\theta_{CAA}/[\theta]$	
			b×h (mm×mm)	ρ (%)	ρ' (%)			d_y	d_{CAA}	θ_y	θ_{CAA}	DoD	GSA	DoD	GSA
This study	P-R	2,750	150×250	0.47	0.70	≤0	NC	30	70	0.0109	0.0145	0.05	0.06	0.29	0.24
	E-R	2,750	150×250	0.47	0.70		NC	20	73	0.0073	0.0193	0.05	0.06	0.39	0.32
Su et al. [2]	A1	1,225	150×300	0.55	0.55	≤0	NC	/	48.0	/	0.0392	0.05	0.06	0.78	0.65
	A2	1,225	150×300	0.83	0.83		C	/	56.4	/	0.0460	0.063	0.1	0.73	0.46
	A3	1,225	150×300	1.13	1.13		C	/	76.4	/	0.0624	0.063	0.1	0.99	0.62
	A4	1,225	150×300	0.38	0.55		NC	/	65.0	/	0.0531	0.05	0.06	1.06	0.89
	A5	1,225	150×300	0.55	0.83		C	/	70.7	/	0.0577	0.063	0.1	0.92	0.58
	A6	1,225	150×300	0.75	1.13		C	/	69.2	/	0.0565	0.063	0.1	0.90	0.57
	B1	1,975	150×300	1.13	1.13		NC	/	100.0	/	0.0506	0.05	0.06	1.01	0.84
	B2	2,725	150×300	1.13	1.13		NC	/	102.0	/	0.0374	0.05	0.06	0.75	0.62
	B3	2,725	150×300	0.75	1.13		NC	/	85.5	/	0.0314	0.05	0.06	0.63	0.52
	C1	1,225	150×200	1.30	1.30		NC	/	33.7	/	0.0275	0.05	0.06	0.55	0.46
Choi and Kim [3]	5G	1,510	185×150	0.66	0.66	≤0	NC	/	84.5	/	0.0560	0.05	0.06	1.12	0.93
	5S	1,505	150×225	0.53	1.31		C	/	103.0	/	0.0684	0.063	0.1	1.09	0.68
	8G	1,510	125×160	0.94	0.94		NC	/	59.0	/	0.0391	0.05	0.06	0.78	0.65
	8S	1,505	140×195	1.00	1.66		C	/	59.3	/	0.0394	0.063	0.1	0.63	0.39
Sadek et al. [4]	IMF	5,385	711×508	0.40	0.63	≤0	C	/	127	/	0.0236	0.063	0.1	0.37	0.24
	SMF	5,233	864×660	0.59	0.69		C	/	112	/	0.0214	0.063	0.1	0.34	0.21
FarhangVesali et al. [5]	1	2,110	180×180	0.59	0.59	≤0	NC	/	49.0	/	0.0232	0.05	0.06	0.46	0.39
	2	2,110	180×180	0.59	0.59		NC	/	44.0	/	0.0209	0.05	0.06	0.42	0.35
	3	2,110	180×180	0.59	0.59		NC	/	50.0	/	0.0237	0.05	0.06	0.47	0.40
	4	2,110	180×180	0.59	0.88		NC	/	54.0	/	0.0256	0.05	0.06	0.51	0.43
	5	2,110	180×180	0.59	0.88		NC	/	54.0	/	0.0256	0.05	0.06	0.51	0.43
	6	2,110	180×180	0.59	0.88		NC	/	52.0	/	0.0246	0.05	0.06	0.49	0.41
Qian and Li [9]	F1	2,175	100×180	0.87	0.87	≤0	NC	13.5	15.4	0.0062	0.0071	0.05	0.06	0.14	0.12
	F2	2,175	100×180	1.47	1.47		NC	15.2	21.3	0.0070	0.0098	0.05	0.06	0.20	0.16
	F3	2,175	100×180	0.87	0.87		NC	7.2	30.0	0.0033	0.0138	0.05	0.06	0.28	0.23
	F4	2,175	100×180	0.87	0.87		NC	16.3	17.8	0.0075	0.0082	0.05	0.06	0.16	0.14
	F5	2,775	240×100	0.65	0.65		NC	20.0	26.1	0.0072	0.0094	0.05	0.06	0.19	0.16
	F6	2,175	100×180	0.87	0.65		NC	17.2	23.5	0.0079	0.0108	0.05	0.06	0.22	0.18
	F7	2,175	100×180	0.87	0.75		NC	13.3	20.2	0.0061	0.0093	0.05	0.06	0.19	0.16
Yu and Tan	S1	2,750	150×250	0.49	0.90	≤0	NC	/	78.0	/	0.0284	0.05	0.06	0.57	0.47

[7]	S2	2,750	150×250	0.49	0.73		NC	/	73.0	/	0.0265	0.05	0.06	0.53	0.44
	S3	2,750	150×250	0.49	1.24		NC	/	74.4	/	0.0271	0.05	0.06	0.54	0.45
	S4	2,750	150×250	0.82	1.24		NC	/	81.0	/	0.0295	0.05	0.06	0.59	0.49
	S5	2,750	150×250	1.24	1.24		NC	/	74.5	/	0.0271	0.05	0.06	0.54	0.45
	S6	2,750	150×250	0.82	1.87		NC	/	114.4	/	0.0416	0.05	0.06	0.83	0.69
	S7	2,150	150×250	0.82	1.24		NC	/	74.4	/	0.0346	0.05	0.06	0.69	0.58
	S8	1,550	150×250	0.82	1.24		NC	/	45.9	/	0.0296	0.05	0.06	0.59	0.49
Yu and Tan [34]	F1-CD	2,750	150×250	0.82	1.24	≤0	NC	/	61.4	/	0.0223	0.05	0.06	0.45	0.37
	F2-MR	2,750	150×250	0.82	1.24		NC	/	87.0	/	0.0316	0.05	0.06	0.63	0.53
	F3-PD	2,750	150×250	0.82	1.24		NC	/	77.4	/	0.0281	0.05	0.06	0.56	0.47
	F4-PH	2,750	150×250	0.90	1.24		NC	/	94.8	/	0.0345	0.05	0.06	0.69	0.58
Kang and Tan [35]	MJ-B-0.52/0.35S	2,750	150×300	0.35	0.52	≤0	C	/	76.7	/	0.0279	0.063	0.1	0.44	0.28
	MJ-L-0.52/0.35S	2,750	150×300	0.35	0.52		C	/	71.8	/	0.0261	0.063	0.1	0.41	0.26
	MJ-B-0.88/0.59R	2,750	150×300	0.59	0.88		C	/	100.9	/	0.0367	0.063	0.1	0.58	0.37
	MJ-L-0.88/0.59R	2,750	150×300	0.59	0.88		C	/	100.9	/	0.0367	0.063	0.1	0.58	0.37
	MJ-L-1.19/0.59R	2,750	150×300	0.59	1.19		C	/	105.7	/	0.0384	0.063	0.1	0.61	0.38
Kang et al. [36]	EMJ-B-1.19/0.59	2,750	150×300	0.59	1.19	≤0	C	/	108.9	/	0.0396	0.063	0.1	0.63	0.40
	EMJ-L-1.19/0.59	2,750	150×300	0.59	1.19		C	/	103.1	/	0.0375	0.063	0.1	0.60	0.38
	EMJ-B-0.88/0.59	2,750	150×300	0.59	0.88		C	/	101.9	/	0.0371	0.063	0.1	0.59	0.37
	EMJ-L-0.88/0.59	2,750	150×300	0.59	0.88		C	/	106.9	/	0.0389	0.063	0.1	0.62	0.39
	EMJ-L-0.88/0.88	2,750	150×300	0.88	0.88		C	/	171.2	/	0.0623	0.063	0.1	0.99	0.62
Qian et al. [37]	P1	1,300	100×180	0.87	0.87	≤0	NC	16.8	37.3	0.0129	0.0158	0.05	0.06	0.32	0.26
	P2	1,300	80×140	1.40	1.40		NC	14.1	30.8	0.0108	0.0128	0.05	0.06	0.26	0.21
Vali pour et al. [10]	No. 1	2,110	180×180	0.59	0.87	≤0	NC	/	59.0	/	0.0260	0.05	0.06	0.52	0.43
	No. 2	2,110	180×180	0.59	0.59		NC	/	54.8	/	0.0260	0.05	0.06	0.52	0.43
	No. 3	2,110	180×180	0.59	0.87		NC	/	55.4	/	0.0263	0.05	0.06	0.53	0.44
	No. 4	2,110	180×180	0.59	0.59		NC	/	56.3	/	0.0267	0.05	0.06	0.53	0.45
Alogla et al. [38]	SS-1	2,775	150×250	0.48	0.72	≤0	NC	57.9	101.0	0.0209	0.0155	0.05	0.06	0.31	0.26
	SS-2	2,775	150×250	0.48	0.72		NC	55.1	96.8	0.0199	0.0150	0.05	0.06	0.30	0.25
	SS-3	2,775	150×250	0.48	0.72		NC	48.2	86.8	0.0174	0.0139	0.05	0.06	0.28	0.23
	SS-4	2,775	150×250	0.48	0.72		NC	60.1	91.4	0.0217	0.0113	0.05	0.06	0.23	0.19
Kang and Tan [12]	EF-B	2,750	150×300	0.59	1.19	≤0	C	/	111.2	/	0.0404	0.063	0.1	0.64	0.40
	EF-L	2,750	150×300	0.59	1.19		C	/	72.1	/	0.0262	0.063	0.1	0.42	0.26
	EF-B-S	2,700	150×300	0.59	1.19		C	/	87.2	/	0.0323	0.063	0.1	0.51	0.32
	EF-L-S	2,700	150×300	0.59	1.19		C	/	78.2	/	0.0290	0.063	0.1	0.46	0.29
Ren et al. [39]	B2	1,900	85×170	0.81	1.04	≤0	NC	/	33.0	/	0.0174	0.05	0.06	0.35	0.29
	B3	1,900	85×200	0.70	0.92		NC	/	33.3	/	0.0175	0.05	0.06	0.35	0.29
Lim et al.	COR	2,220	100×180	1.02	1.53	≤0	NC	/	108	/	0.0486	0.05	0.06	0.97	0.81

[40]	EXT	2,220	100×180	1.02	1.53		NC	/	108	/	0.0486	0.05	0.06	0.97	0.81
Lim et al. [41]	FR	2,400	100×180	1.01	1.52	≤0	NC	46	84	0.0192	0.0158	0.05	0.06	0.32	0.26
	FR-S	2,400	100×180	1.01	1.52		C	45	95	0.0188	0.0208	0.063	0.1	0.33	0.21
	FR-R	2,400	100×180	1.33	2.02		C	34	70	0.0142	0.0150	0.063	0.1	0.24	0.15
	IR-1	2,400	100×180	1.01	1.52		NC	46	89	0.0192	0.0179	0.05	0.06	0.36	0.30
	IR-2	2,400	100×180	1.01	1.52		NC	53	70	0.0221	0.0071	0.05	0.06	0.14	0.12
Yu and Tan [13]	F2-WS	2,750	150×250	0.82	1.24	≤0	NC	/	84.8	/	0.0308	0.05	0.06	0.62	0.51
	F3-NS-H	2,750	150×250	0.82	1.24		NC	/	84.4	/	0.0307	0.05	0.06	0.61	0.51
	F4-WS-H	2,750	150×250	0.82	1.24		NC	/	84.4	/	0.0307	0.05	0.06	0.61	0.51
Deng et al. [11]	NSC-8	2,000	150×250	0.67	1.01	≤0	NC	25	79	0.0125	0.0270	0.05	0.06	0.54	0.45
	NSC-11	2,750	150×250	0.67	1.01		NC	36	90	0.0131	0.0196	0.05	0.06	0.39	0.33
	NSC-13	3,250	150×250	0.67	1.01		NC	45	108	0.0138	0.0194	0.05	0.06	0.39	0.32
	HSC-8	2,000	150×250	0.67	1.01		NC	16	80	0.0080	0.0320	0.05	0.06	0.64	0.53
	HSC-11	2,750	150×250	0.67	1.01		NC	28	74	0.0102	0.0167	0.05	0.06	0.33	0.28
	HSC-13	3,250	150×250	0.67	1.01		NC	35	104	0.0108	0.0212	0.05	0.06	0.42	0.35
Diao et al. [42]	OP	2,250	100×250	0.70	0.70	≤0	NC	18	65	0.0080	0.0209	0.05	0.06	0.42	0.35
	OA	2,250	100×250	0.70	0.70		NC	15	50	0.0067	0.0156	0.05	0.06	0.31	0.26
	TP	2,250	100×250	0.70	0.70		NC	15	91	0.0067	0.0338	0.05	0.06	0.68	0.56
Feng et al. [43]	PCF-1	2,600	150×250	0.69	1.24	≤0	C	/	79.2	/	0.0305	0.063	0.1	0.48	0.31
	PCF-2	2,600	180×300	0.37	0.65		C	/	79.2	/	0.0305	0.063	0.1	0.48	0.31
	PCF-3	2,600	180×300	0.37	0.65		C	/	93.4	/	0.0359	0.063	0.1	0.57	0.36
	PCF-4	2,600	150×250	0.69	1.24		C	/	86.2	/	0.0332	0.063	0.1	0.53	0.33
Zhang et al. [44]	PC-H	3,600	200×420	0.50	0.75	≤0	C	18.1	86.0	0.0050	0.0189	0.063	0.1	0.30	0.19
	PC-L	3,600	200×420	0.64	0.75		C	41.6	81.6	0.0116	0.0111	0.063	0.1	0.18	0.11
	PC-A	3,600	200×420	0.50	0.75		C	20.6	90.2	0.0057	0.0193	0.063	0.1	0.31	0.19
Gu et al. [45]	B1A	1,800	100×150	0.80	0.80	≤0	NC	39.6	50.9	0.0220	0.0063	0.05	0.06	0.13	0.11
	B1	1,800	100×150	0.80	0.80		NC	26.7	63.9	0.0148	0.0207	0.05	0.06	0.41	0.35
	TB3	1,800	100×150	0.80	0.80		NC	12.9	64.2	0.0072	0.0285	0.05	0.06	0.57	0.48
	TB4	1,800	100×150	0.80	0.80		NC	13.3	70.5	0.0074	0.0318	0.05	0.06	0.64	0.53
	TB5	1,800	100×150	0.80	0.80		NC	27.1	56.5	0.0151	0.0163	0.05	0.06	0.33	0.27
Long et al. [46]	FN-1.05	2,450	150×250	0.67	1.01	≤0	NC	/	80	/	0.0327	0.05	0.06	0.65	0.55
	FS-1.05	2,450	150×250	0.67	1.01		C	/	102	/	0.0416	0.063	0.1	0.66	0.42
	FS-1.43	2,450	150×250	0.67	1.37		C	/	95	/	0.0388	0.063	0.1	0.62	0.39
	FS-1.43E	2,450	150×250	0.67	1.37		C	/	76	/	0.0310	0.063	0.1	0.49	0.31
	FS-1.86E	2,450	150×250	0.67	1.79		C	/	68	/	0.0278	0.063	0.1	0.44	0.28
Qian et al. [47]	IA	2,750	150×250	0.67	1.01	≤0	NC	46	68	0.0167	0.0080	0.05	0.06	0.16	0.13
	SA	2,750	150×250	0.67	1.01		NC	31	66	0.0113	0.0127	0.05	0.06	0.25	0.21
	UB	2,750	150×250	0.67	1.01		NC	36	76	0.0131	0.0145	0.05	0.06	0.29	0.24

Qian et al. [48]	SL-8	2,000	150×250	0.67	1.01	0.119	NC	23	80	0.0115	0.0285	0.044	0.053	0.65	0.54
	SL-11	2,750	150×250	0.67	1.01	0.119	NC	35	90	0.0127	0.0200	0.044	0.053	0.45	0.38
	SL-13	3,250	150×250	0.67	1.01	0.119	NC	43	100	0.0132	0.0175	0.044	0.053	0.40	0.33
Qian et al. [49]	RCM	2,750	150×250	0.67	1.01	≤ 0	NC	30	70	0.0109	0.0145	0.05	0.06	0.29	0.24
	RCP	2,750	150×250	0.67	1.01		NC	27	76	0.0098	0.0178	0.05	0.06	0.36	0.30

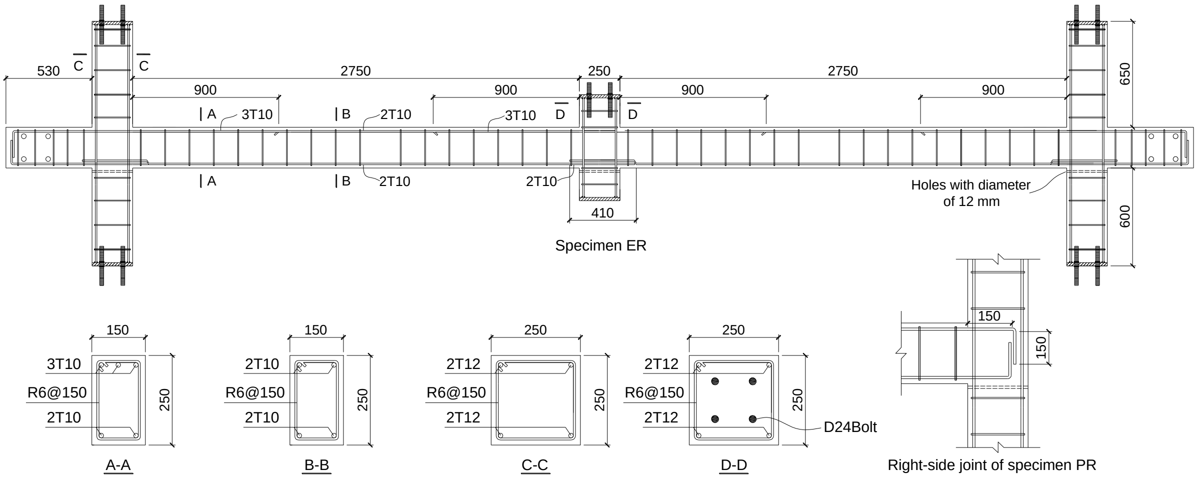

Fig. 1 Geometric dimension and reinforcement arrangement of sub-frames

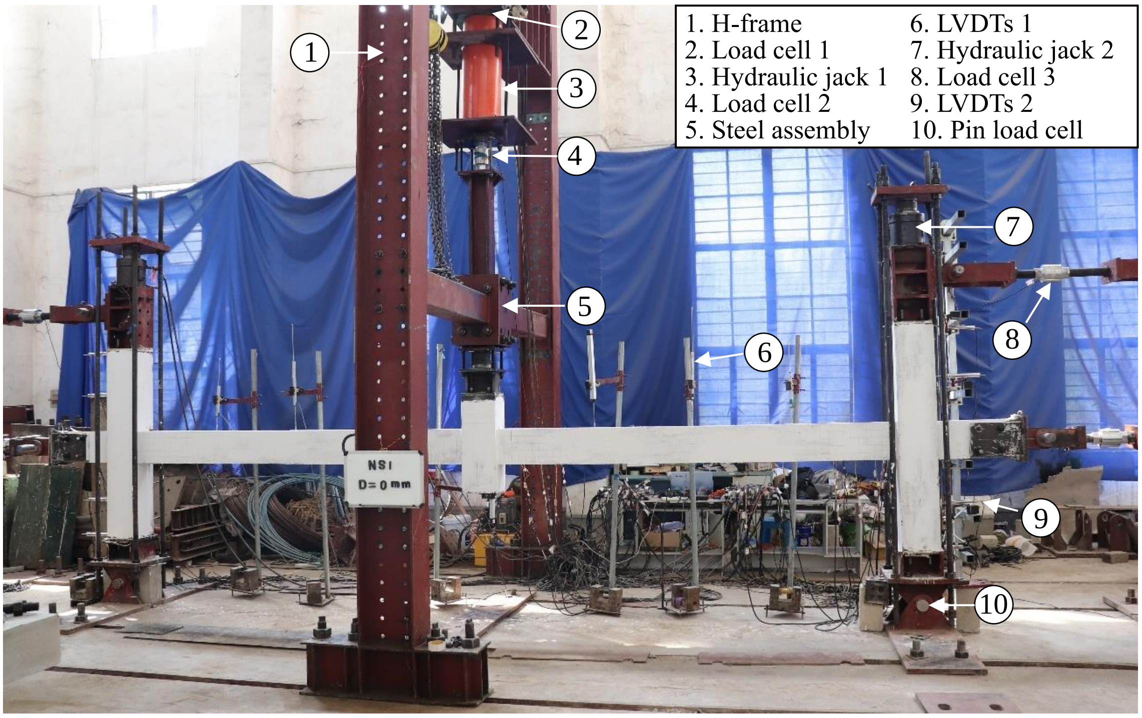

Fig. 2 Test setup

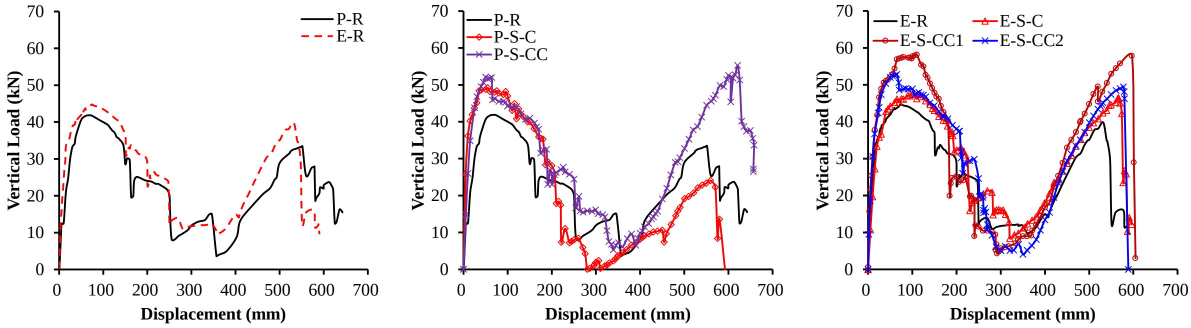

(a) (b) (c)

Fig. 3 Load resistance-displacement history: (a) referential sub-frames; (b) P-series sub-frames; (c) E-series sub-frames

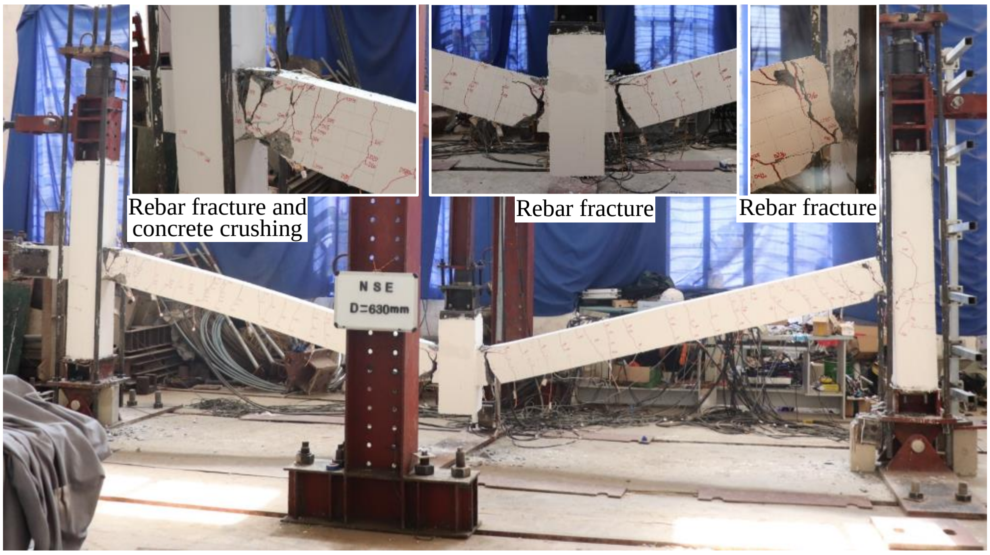

Fig. 4 Failure mode of P-R

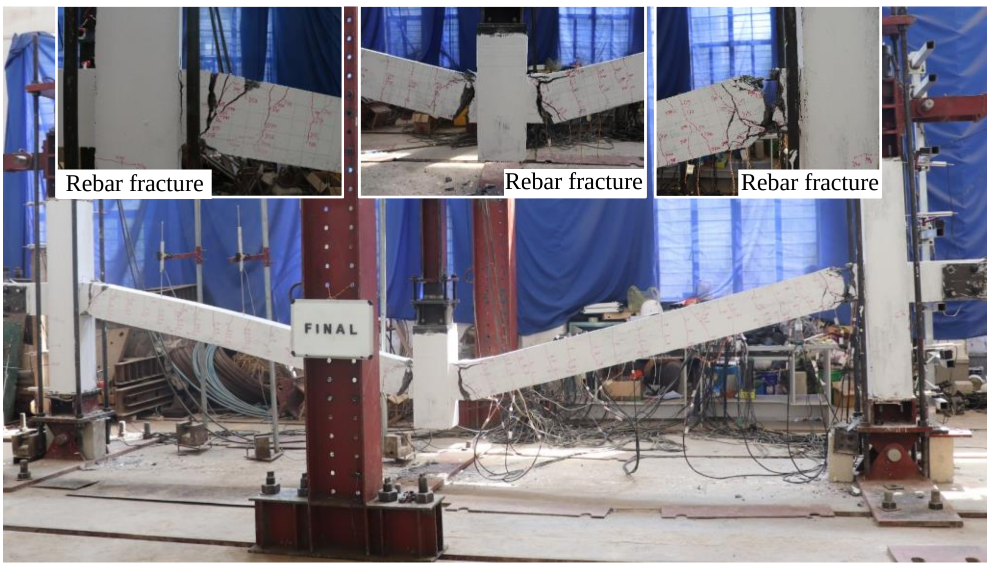

Fig. 5 Failure mode of E-R

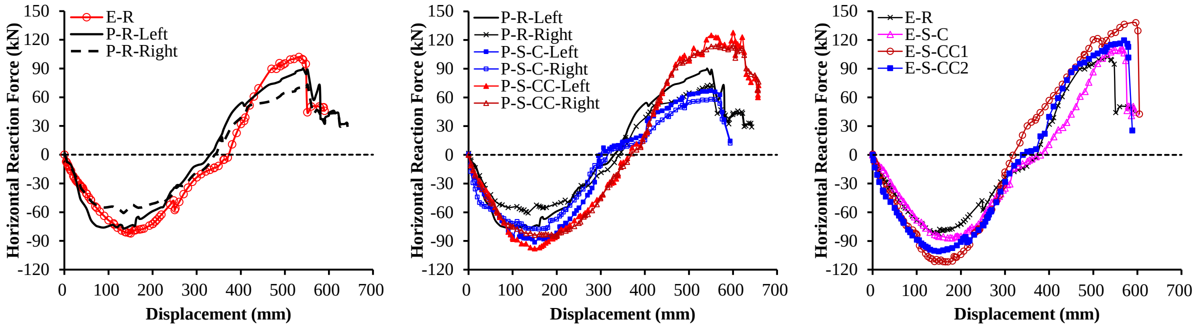

(a) (b) (c)

Fig. 6 Horizontal reaction force-displacement history: (a) referential sub-frames; (b) P-series sub-frames; (c) E-series sub-frames

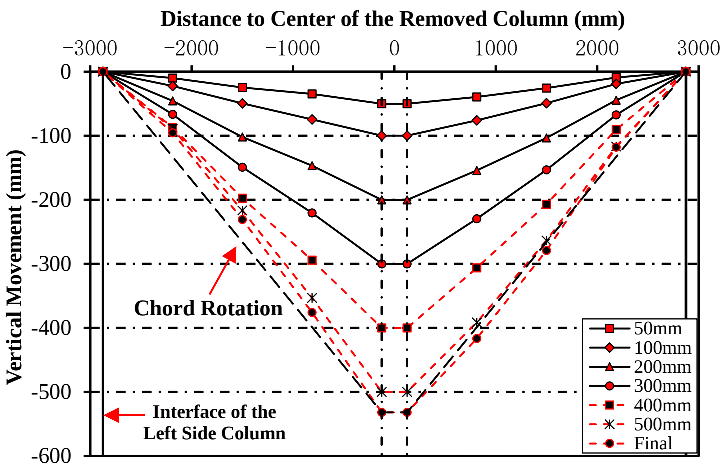

Fig. 7 Beam deflection of E-R

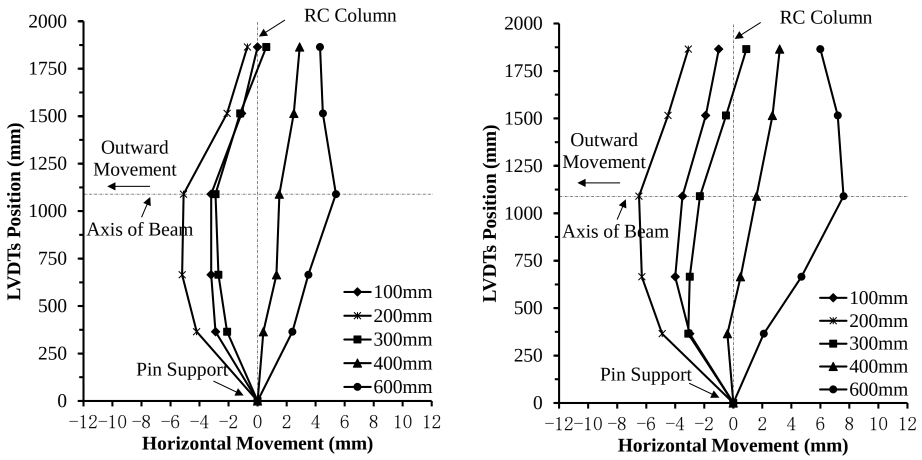

(a) (b)

Fig. 8 Deflection of the right side column: (a) E-R; (b) P-R

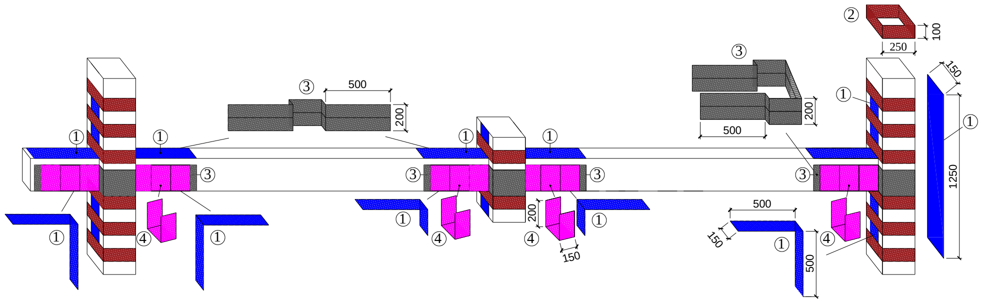

(a)

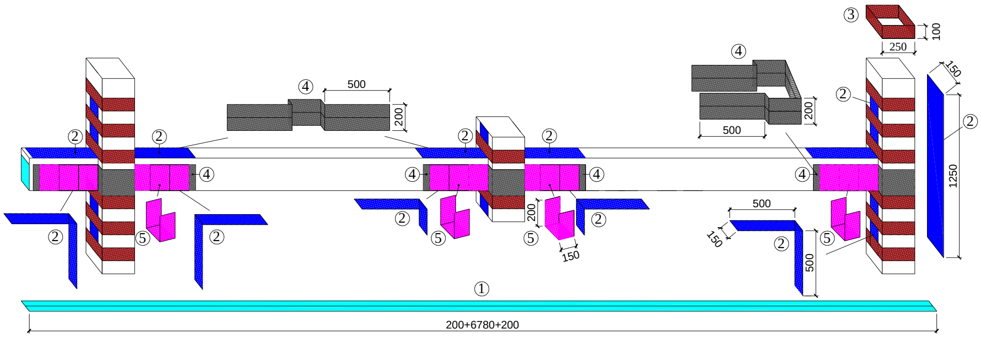

(b)

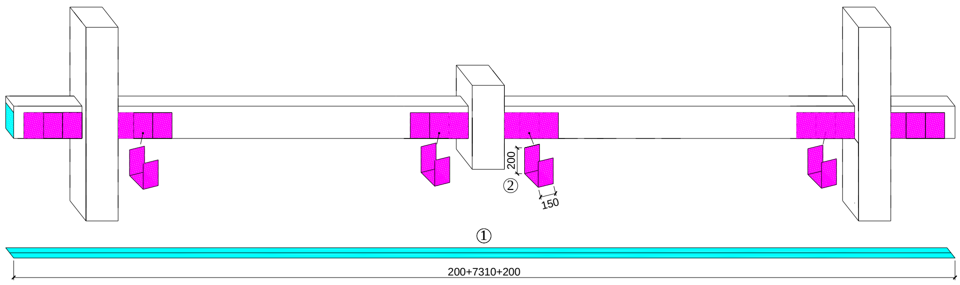

(c)

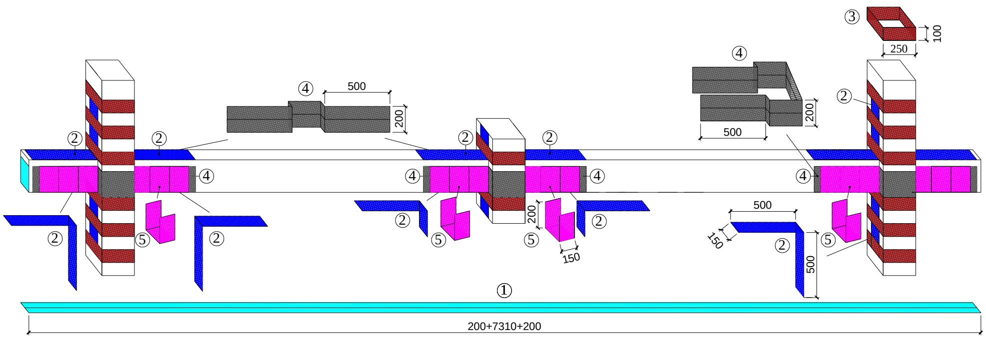

(d)

Fig. 9 Strengthening scheme of sub-frames: (a) P-S-C; (b) P-S-CC; (c) E-S-C;(d) E-S-CC1& E-S-CC2

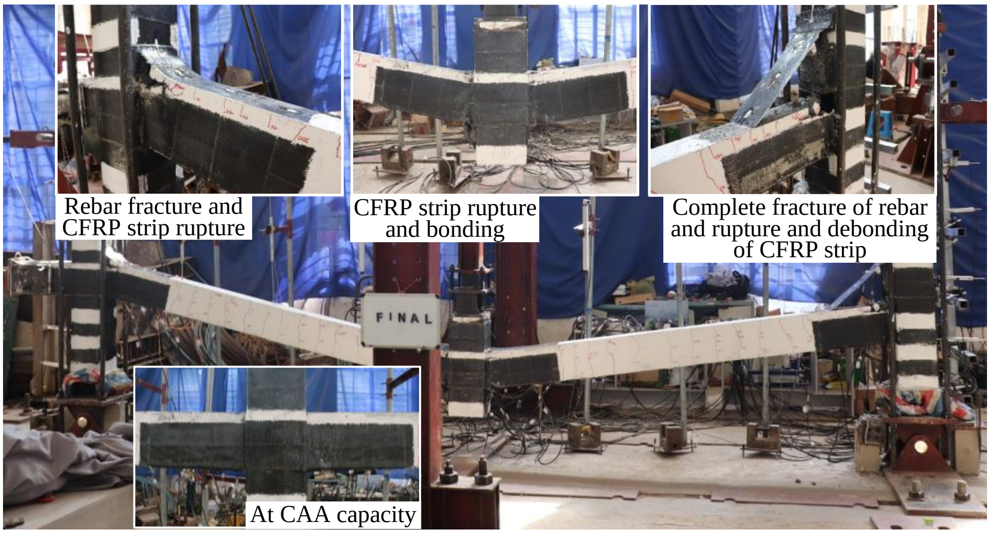

Fig. 10 Failure mode of P-S-C

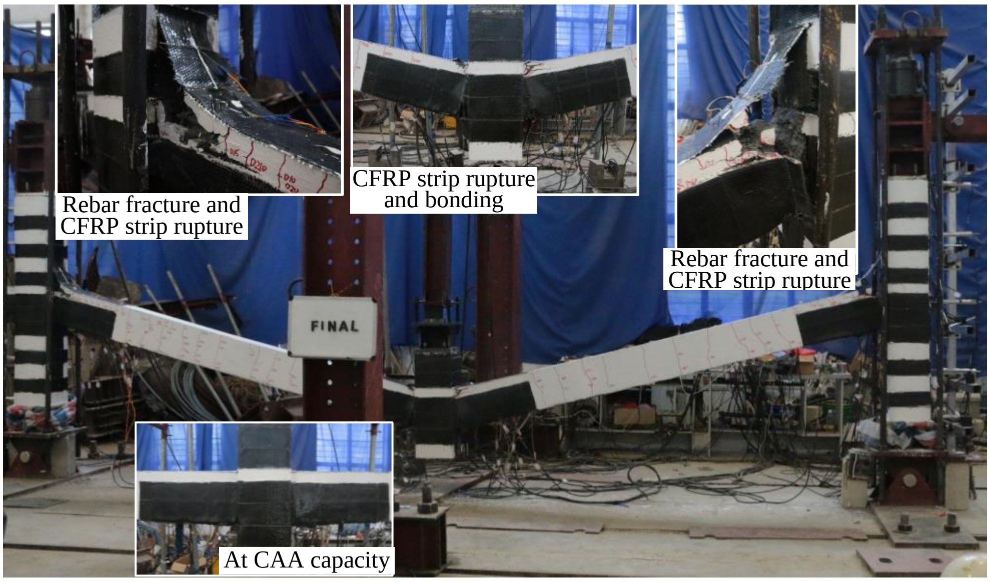

Fig. 11 Failure mode of P-S-CC

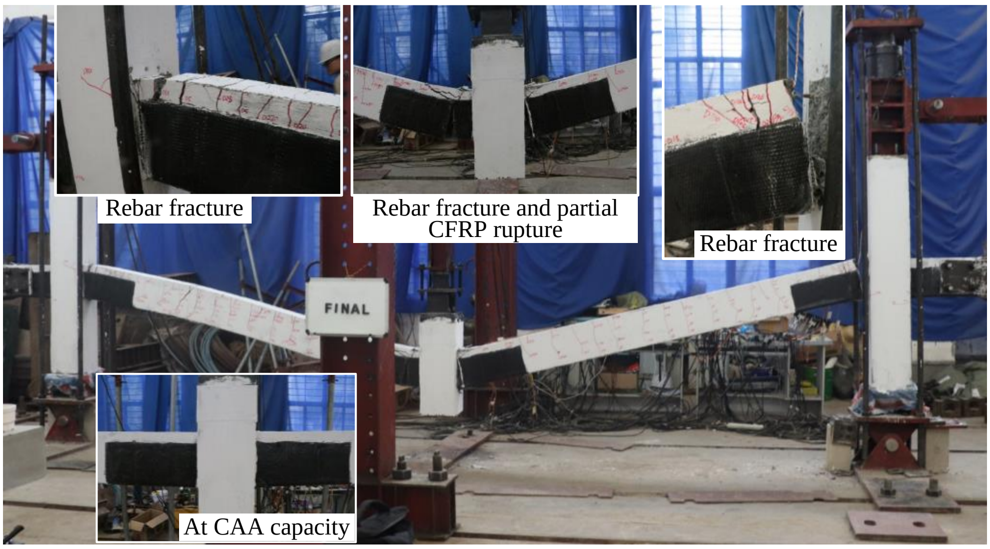

Fig. 12 Failure mode of E-S-C

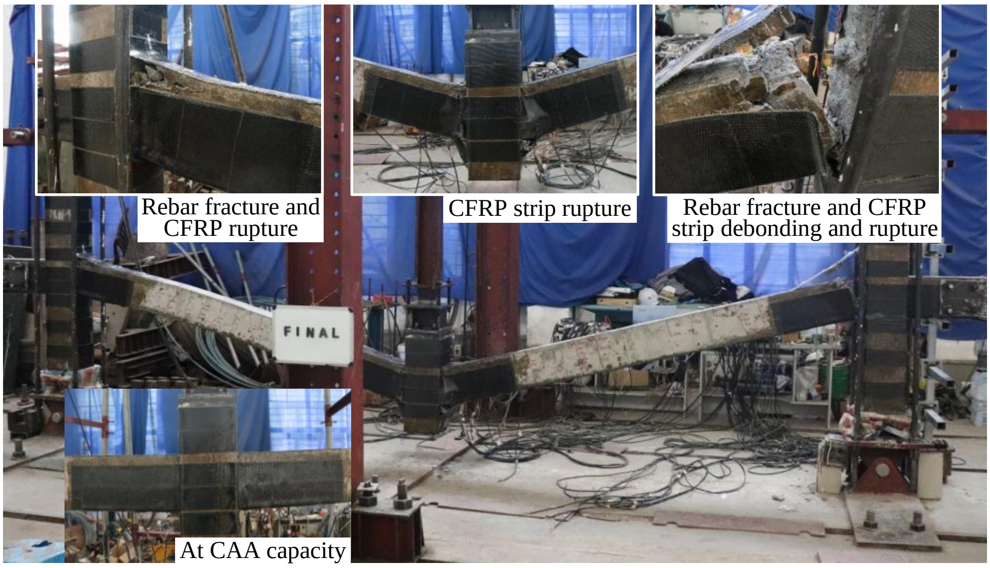

Fig. 13 Failure mode of E-S-CC1

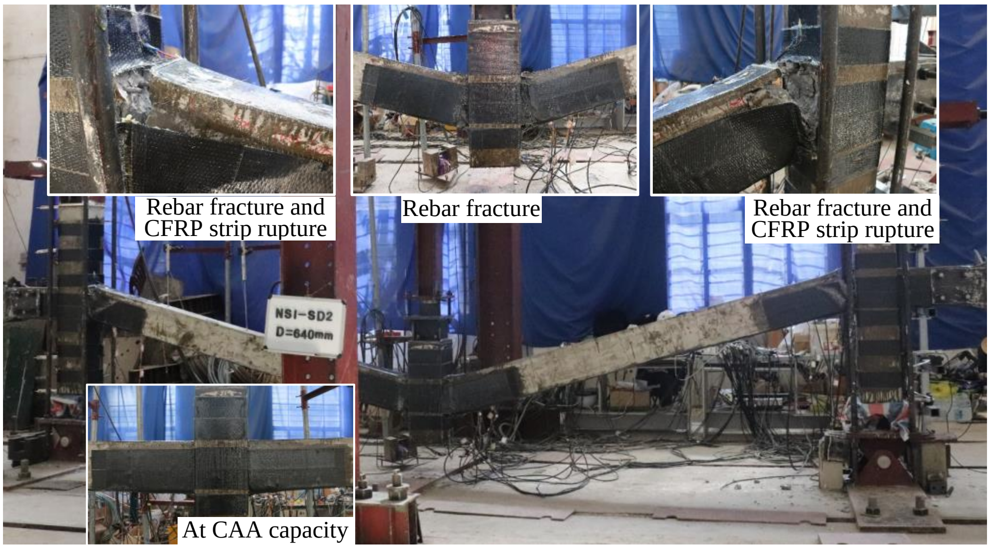

Fig. 14 Failure mode of E-S-CC2

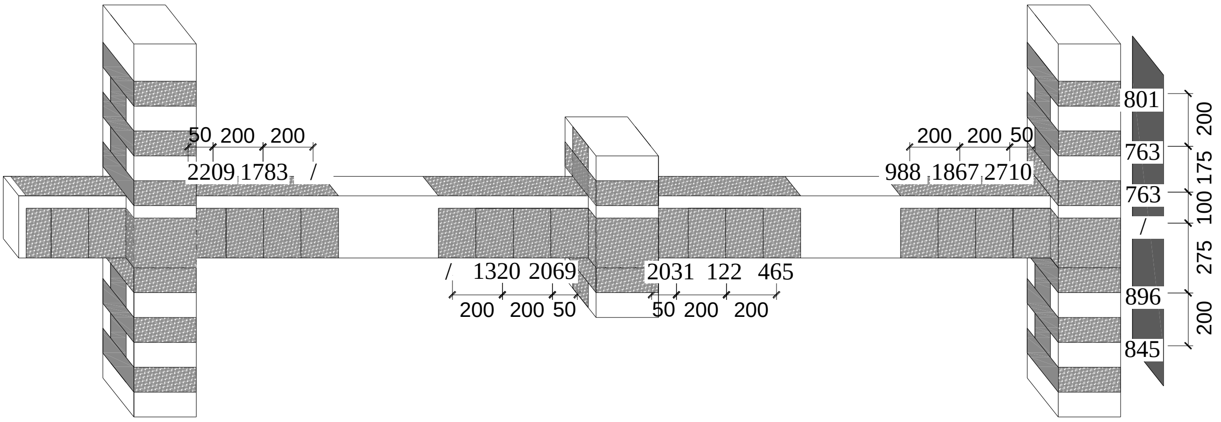

(a)

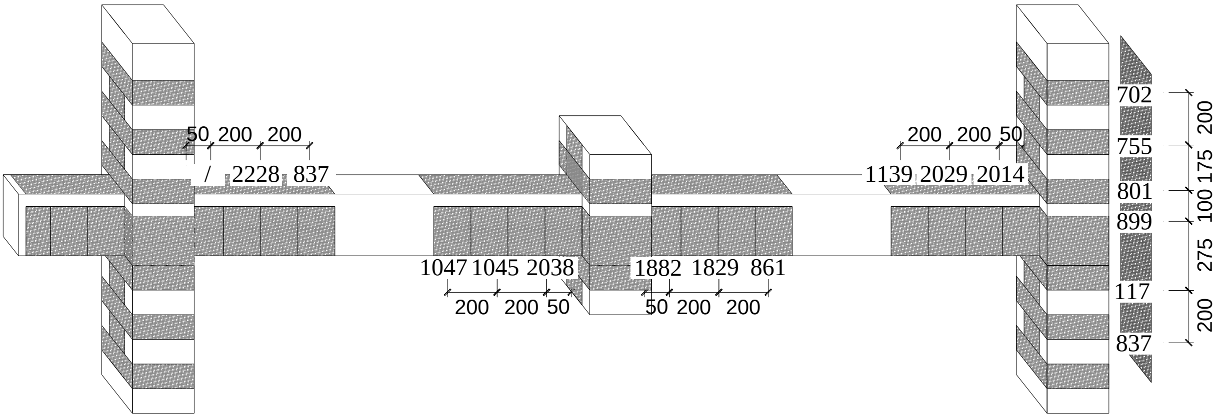

(b)

Fig. 15 Strain of CFRP strips at CAA capacity: (a) P-S-C; (b) P-S-CC (unit in με)

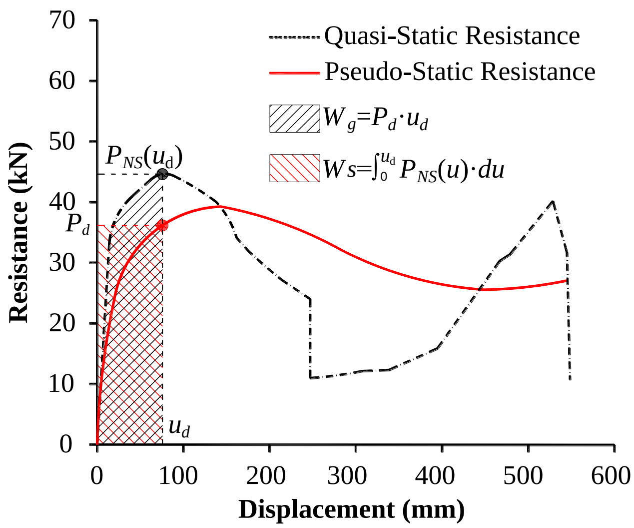

Fig. 16 Illustration of the energy-based method

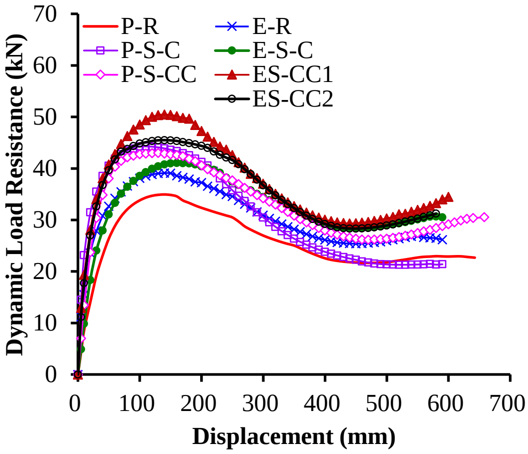

Fig. 17 Dynamic collapse-resistant capacity of the sub-frames

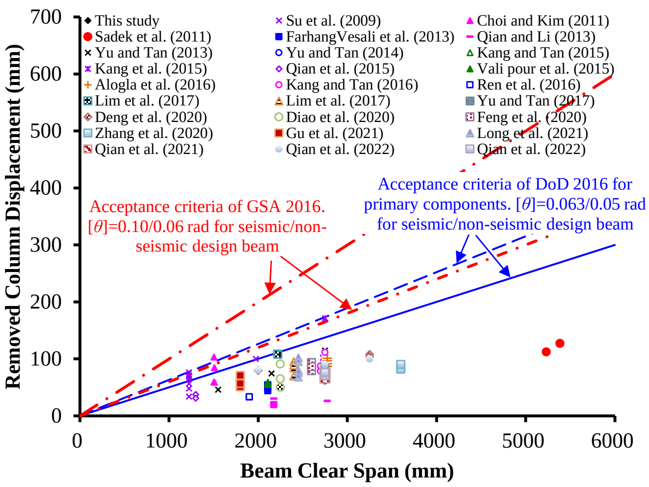

Fig. 18 Comparison of the measured plastic rotations at CAA capacity with the acceptable ones

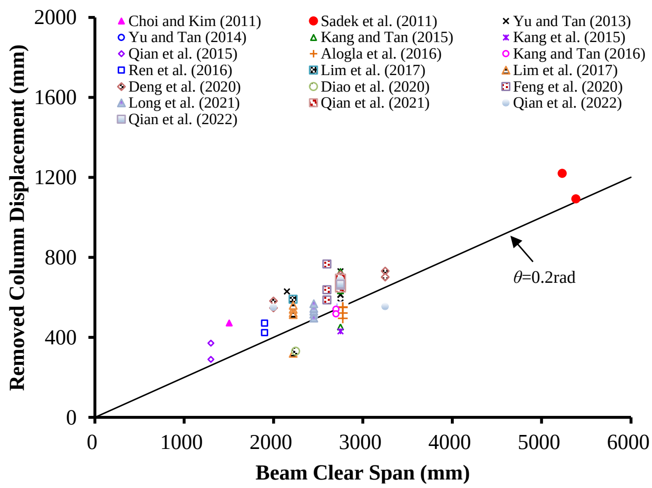

Fig. 19 Measured plastic rotations at CA capacity for the beams with considerable CA capacities

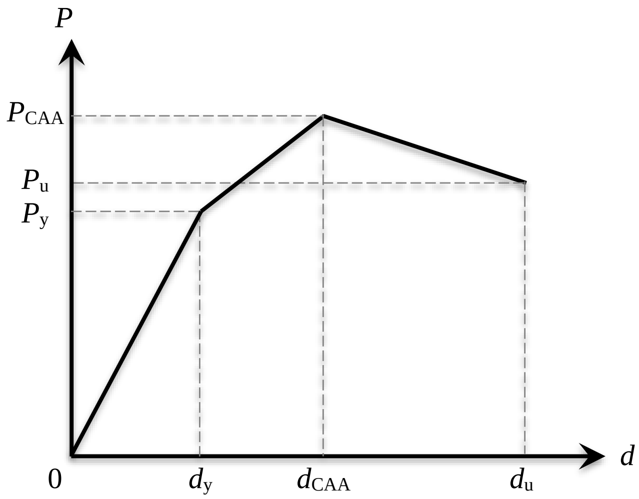

Fig. 20 Proposed load resistance function